Energy 166 (2019) 256–266

Contents lists available at ScienceDirect

Energy

journal homepage: www.elsevier.com/locate/energy

# Thermodynamic and optical analyses of a hybrid solar CPV/T system with high solar concentrating uniformity based on spectral beam splitting technology

Gang Wang [a, *], Yubo Yao [a], Zeshao Chen [b], Peng Hu [b]

[a] School of Energy and Power Engineering, Northeast Electric Power University, Jilin, Jilin 132012, China
[b] University of Science and Technology of China, Hefei, Anhui 230027, China

ARTICLE INFO

*Article history:*
Received 8 August 2018
Received in revised form
13 October 2018
Accepted 15 October 2018
Available online 16 October 2018

*Keywords:*
Hybrid solar CPV/T system
High solar concentrating uniformity
Spectral beam splitting technology
Thermodynamic analysis
Optical analysis

ABSTRACT

A novel multi-segment mirror hybrid solar concentration photovoltaic/thermal (CPV/T) system using the spectral beam splitting technology is proposed, and its composition, working principle and structural design method are introduced in this paper. The Needle optimization method is employed to design the spectral beam splitter for the CPV/T system. The Monte Carlo Ray Tracing method is used to simulate the solar concentrating process and the results reveal that the CPV/T system can provide high uniformity of solar radiation flux density distribution on solar cells. The relationships of key structural and optical parameters of the CPV/T system are investigated. The results indicate that increasing the solar cell installation height and reducing the solar cell width can both improve the geometric concentration ratio of the CPV/T system. The sun tracking error effect analysis is carried out. The analysis results indicate that the CPV/T system has an overall optical efficiency higher than 76.3% when the sun tracking error is less than 1°. Furthermore, the thermodynamic analysis of the proposed CPV/T system is conducted and the results show that the PV conversion efficiency and overall energy efficiency of the CPV/T system are both higher than those of the CPV system under the same condition.



## 1. Introduction

Solar energy is clean, plentiful and commonly considered as one of the most viable types of renewable energy sources. It has good prospects for sustainable development and utilization in the future. Two major applications of solar energy are the solar thermal and photovoltaic (PV) power generations, respectively. Solar thermal power generation is designed to generate steam and then produce current by using the steam turbine, while solar PV cells convert solar radiation directly into electricity [1–3]. As the conversion efficiency of commercialized solar PV power generation is still low and the cost is high, the solar PV system is limited in actual applications. One of the high cost factors of solar power generation comes from the high cost of solar cells, and the method of solar concentration can effectively reduce the cost of solar PV power generation as it could decrease the amount of solar cells [4–6]. A solar concentrator with a higher concentration uniformity will be good for improving the photo-electric conversion efficiency [5,7–9]. In addition, as there is a spectral response for a solar cell, not all the solar radiation energy could be used for electrical power production. The part of solar energy dissipated as heat would cause the temperature increase of solar cells, leading to the decrease of the photo-electric conversion efficiency. A good designed hybrid solar concentration photovoltaic/thermal (CPV/T) system could solve this problem to a certain extent [10–12]. The heat removed by the working medium in the thermal collector (or the cooling system) could be used in other aspects (e.g., the seawater desalination, the hydrogen production or the hot water supply), which will not only decrease the solar cell temperature but also increase the overall utilization efficiency of solar energy [13].

Many research works on the hybrid solar CPV/T systems have been conducted and some typical studies are presented as follows. A two-stage solar CPV/T system based on the parabolic trough was proposed by Jiang et al. [10]. The spectral beam splitter was specially designed and the theoretical overall optical efficiency was approximately 76.4%. Another typical solar CPV/T system was design by Liu et al. [11]. It was based on the linear Fresnel reflector (LFR) and also used a spectral beam splitting filter. The

* Corresponding author.
*E-mail address:* kinggang009@163.com (G. Wang).

https://doi.org/10.1016/j.energy.2018.10.089
0360-5442/

thermodynamic and optical analyses of the CPV/T system were carried out and the results showed that the energy efficiency was higher in comparison with the CPV system. Lasich et al. [14] proposed a solar CPV/T system which was comprised of a parabolic dish, a secondary concentrator, a light guide and a flux modifier. Relevant experiments were carried out and the results revealed that the total cogeneration efficiency was 31.8%. A CPV/T prototype using the nanofluid absorption filter was built by Crisostomo et al. [15]. The experimental results indicated that the nanofluid of 0.027 wt% Ag could lead to an 11% increase of the combined output in comparison with water. A comprehensive review on hybrid solar CPV/T systems using spectral beam splitter was carried out by Ju et al. [12]. Many kinds of spectral beam splitting technologies and typical hybrid solar CPV/T system designs were introduced, and the advantages and disadvantages of different spectral beam splitting technologies were summarized in this review article.

In this paper, a novel hybrid solar CPV/T system with spectral beam splitter is proposed. The system design is based on a multi-segment mirror solar concentrator so that the solar concentration uniformity would be relatively higher than those of traditional concentrators (e.g., the parabolic dish and parabolic trough concentrators) [7]. The design principle of the proposed CPV/T system is provided and the spectral beam splitter used in this system is designed. The simulation of the solar concentrating process and sun tracking error effect analysis are carried out. And the optical and thermodynamic analyses of the CPV/T system are also conducted.

## 2. Design of the hybrid solar CPV/T system

The layout of the multi-segment mirror hybrid solar CPV/T system is presented in Fig. 1. The system mainly includes a reflective solar concentrator comprised of some flat mirrors connected end to end, a spectral beam splitter, some solar cells, a solar thermal receiver tube collector and a secondary reflector. When the sunlight is incident vertically onto the CPV/T system, the solar ray will be reflected by the flat mirror array to the solar cell surfaces, forming a relatively uniform solar radiation distribution on them. The solar cells are plated with a coating system, which is used as the spectral beam splitter. In this CPV/T system, when the concentrated solar ray is incident on the spectral beam splitter, part of it passes through the beam splitter and then will be converted to electricity by solar cells, and the other part is reflected to the solar thermal receiver tube collector. Some deviated light will be re-reflected onto the receiver tube by the secondary reflector. The solar energy reflected onto the receiver tube surface will be partly absorbed by the heat-transfer medium in the tube collector and then used for hot water supply, driving absorption refrigeration, thermal power generation or other utilizations according to the demands of different users. In order to make the incident solar ray perpendicular to the horizontal plane of the system bracket, the system should be equipped with a two-axis sun tracker.

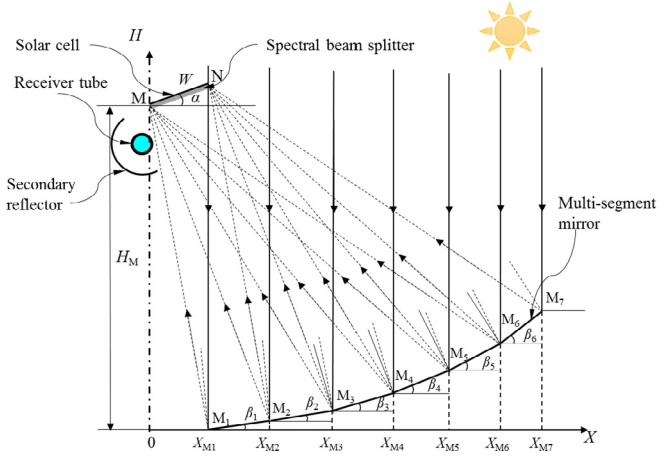


**Fig. 1.** Layout of the multi-segment mirror hybrid solar CPV/T system.

### 2.1. Design of the solar concentrator

As shown in Fig. 1, it is the structural diagram of the multi-segment mirror hybrid solar CPV/T system. MN represents a solar cell with a tilt angle $\alpha$, in which M and N are the two boundary points, respectively. The concentrated solar energy flux density should distribute uniformly between the two points. In the flat mirror array, $M_i$ and $M_{i+1}$ are the starting and end points of the $i$-th flat mirror, respectively. $\beta_i$ and $K_i$ are the tilt angle and slope of the $i$-th flat mirror and there should be $K_i = \tan\beta_i$. $H_M$ and $W$ stand for the installing height and width of the solar panel, respectively. To utilize the area of incident sunlight maximally, the starting point $M_1$ of the first flat mirror and point N have the same $X$-axis value, and all flat mirrors are connected end to end. For the $X$-$H$ coordinate system, there are $X_M = 0$ , $X_N = W\cos\alpha$ and $H_N = H_M + W\sin\alpha$. It can be derived that the position equation of the solar panel is:

$$H = K_{MN}(X - X_M) + H_M \tag{1}$$

where, there is $K_{MN} = \tan\alpha$. The horizontal and vertical coordinate values of $M_1$ of the first flat mirror are $X_{M1} = W\cos\alpha$ and $H_{M1} = 0$, respectively.

The slope and equation of the first flat mirror could be calculated as follows:

$$K_1 = \tan\beta_1 = \frac{H_{M_1} - H_M}{X_{M_1}} + \sqrt{\left(\frac{H_{M_1} - H_M}{X_{M_1}}\right)^2 + 1} \tag{2}$$

$$H = K_1(X - W\cos\alpha) \tag{3}$$

Therefore, the horizontal and vertical coordinates of the end point $M_2$ of the first flat mirror can be obtained:

$$X_{M_2} = \frac{(MM_1 + W\sin\alpha)X_{M_1} - (H_{M_1} - H_M)W\cos\alpha}{MM_1} \tag{4}$$

$$\begin{aligned} H_{M_2} = {} & \frac{(H_{M_1} - H_M)(MM_1 + H_{M_1} - H_M)\left(1 - \frac{W\cos\alpha}{X_{M_1}}\right)}{MM_1} \\ & - \frac{(H_{M_1} - H_M)H_{M_1}}{MM_1} \\ & + \frac{(MM_1 + H_{M_1} - H_M)(H_M + W\sin\alpha)}{MM_1} \end{aligned} \tag{5}$$

In Eqs. (4) and (5), there is $MM_1 = \sqrt{(H_M - H_{M_1})^2 + X_{M_1}^2}$. $MM_1$ represents the distance between points M and $M_1$. Similarly, for the $i$-th flat mirror, its slope and the coordinate values of its end point (i.e., the starting point of the $(i + 1)$-th flat mirror) could be expressed as:

$$K_i = \frac{H_{M_i} - H_M}{X_{M_i}} + \sqrt{\left(\frac{H_{M_i} - H_M}{X_{M_i}}\right)^2 + 1} \tag{6}$$

$$X_{M_{i+1}} = \frac{(MM_i + W\sin\alpha)X_{M_i} - (H_{M_i} - H_M)W\cos\alpha}{MM_i} \tag{7}$$

$$H_{M_{i+1}} = \frac{(H_{M_i} - H_M)(MM_i + H_{M_i} - H_M)\left(1 - \frac{W\cos\alpha}{X_{M_i}}\right)}{MM_i} - \frac{(H_{M_i} - H_M)H_{M_i}}{MM_i} + \frac{(MM_i + H_{M_i} - H_M)(H_M + W\sin\alpha)}{MM_i} \tag{8}$$

where, there is $MM_i = \sqrt{(H_M - H_{M_i})^2 + X_{M_i}^2}$. $MM_i$ stands for the distance between points M and $M_i$. And according to Eqs. (6)–(8), the width $L_i$ of the $i$-th flat mirror can be calculated as:

$$L_i = \sqrt{1 + K_i^2}(X_{M_{i+1}} - X_{M_i}) \tag{9}$$

Based on the nine equations above, the structural parameters of the solar concentrator could be determined. The theoretical geometric concentration ratio ($CR$) of the hybrid solar CPV/T system is defined as the ratio of the solar cell width and the solar concentrator width:

$$CR = \frac{X_{M_N} - X_{M_1}}{W} \tag{10-a}$$

Meanwhile, the relative aperture $AR$ of the hybrid solar CPV/T system is defined as:

$$AR = \frac{X_{M_N}}{H_M} \tag{10-b}$$

In the following simulation of solar concentrating process of the hybrid solar CPV/T system, the size of solar cell is assumed to be 100 mm × 300 mm. Hence, the width of the solar cell is 100 mm. $H_M$ and $\alpha$ are assumed to be 800 mm and 0°, respectively. According to the equations and assumptions above, the structural design results of the solar concentrator are obtained and presented in Table 1.

As the flat mirrors of the solar concentrator are connected end to end, the light loss caused by the mirror thickness is small, and that should be considered in the actual processing. On the whole, this kind of hybrid solar CPV/T system is simple and convenient. The structure materials are easy to obtain, the cost is low, and the processing precision requirement is not high. Thus, it is suitable for the large-scale development and application.

**Table 1**
Structure design results of the concentrator of hybrid solar CPV/T system.

| $i$ | $\beta_i$ | $K_i$ | $L_i$ | $CR$ | $AR$ |
|---|---|---|---|---|---|
| 1 | 3.09 | 0.05 | 99.56 | 0.99 | 0.23 |
| 2 | 6.59 | 0.12 | 98.01 | 1.97 | 0.35 |
| 3 | 9.94 | 0.18 | 95.47 | 2.91 | 0.47 |
| 4 | 13.10 | 0.23 | 92.12 | 3.81 | 0.58 |
| 5 | 16.03 | 0.29 | 88.18 | 4.65 | 0.69 |
| 6 | 18.70 | 0.34 | 83.86 | 5.45 | 0.79 |
| 7 | 21.13 | 0.39 | 79.34 | 6.19 | 0.88 |
| 8 | 23.32 | 0.43 | 74.77 | 6.87 | 0.97 |
| 9 | 25.28 | 0.47 | 70.25 | 7.51 | 1.05 |
| 10 | 27.04 | 0.51 | 65.86 | 8.10 | 1.12 |
| 11 | 28.62 | 0.55 | 61.64 | 8.64 | 1.19 |
| 12 | 30.03 | 0.58 | 57.63 | 9.14 | 1.25 |
| 13 | 31.30 | 0.61 | 53.85 | 9.60 | 1.31 |
| 14 | 32.45 | 0.64 | 50.28 | 10.02 | 1.36 |
| 15 | 33.47 | 0.66 | 46.95 | 10.41 | 1.41 |

### 2.2. Design of the spectral beam splitter

The spectral beam filter is an important element in the CPV/T system [16,17]. The spectral beam splitter used in this multi-segment mirror hybrid solar CPV/T system is a spectrally selective coating system which is plated on the surfaces of solar cells. For this hybrid solar CPV/T system design, as single crystalline silicon (c-Si) solar cells are employed, the theoretical spectral reflectivity of the ideal spectrally selective coating system should be:

$$\rho(\lambda) = \begin{cases} 0 & (380\text{nm} \le \lambda \le 1100\text{nm}) \\ 1 & (\lambda < 380\text{nm}, \lambda > 1100\text{nm}) \end{cases} \tag{11}$$

where $\lambda$ is the wavelength of sunlight. In this study, the Needle optimization method is employed to design the coating system [18]. For the Needle optimization method, the objective function (or merit function) is [19]:

$$MF = \left\{ \frac{1}{N}\sum_{j=1}^{N}\left[\frac{f(\lambda_j) - f_j'}{\Delta f_j}\right]^2 \right\}^{1/2} \tag{12}$$

where $f(\lambda_j)$ is the actual spectral characteristic (reflectivity or transmissivity), and $\lambda_j$ are wavelength points from a given wavelength grid with the total number of $N$ points. $f_j'$ are target values and $\Delta f_j$ stands for the specified tolerance. The optimization design process is searching a suitable coating system structure by constantly inserting new thin films into the coating system and reducing the objective function value.

$Nb_2O_3$ and $Na_3AlF_6$ are chosen as the high refractive index materials, and Ge is used as the low refractive index material. The design targets should be as follows: $\rho(\lambda) = 0$ for the spectral range from 380 nm to 1100 nm, and $\rho(\lambda) = 1$ for other wavelengths. A comparison of design results of the coating systems with different layer numbers is presented in Fig. 2.

Considering the solar energy spectrum distribution and the processing complexity of coating system, the final design structure of the multi-layered film is chosen to be the one with 13 layers, which is specified as follows:

A $177.22H_1$ $56.43H_2$ 72.19L $56.43H_2$ $177.22H_1$ $56.43H_2$ 72.19L $56.43H_2$ $177.22H_1$ $56.43H_2$ 72.19L $56.43H_2$ $88.61H_1$ G where A represents the ambient medium (air), G stands for the base material (c-Si solar cell), $H_1$ is $Na_3AlF_6$, $H_2$ is $Nb_2O_3$, and L is Ge. The spectral reflectivity curves of the ideal and optimized spectral beam

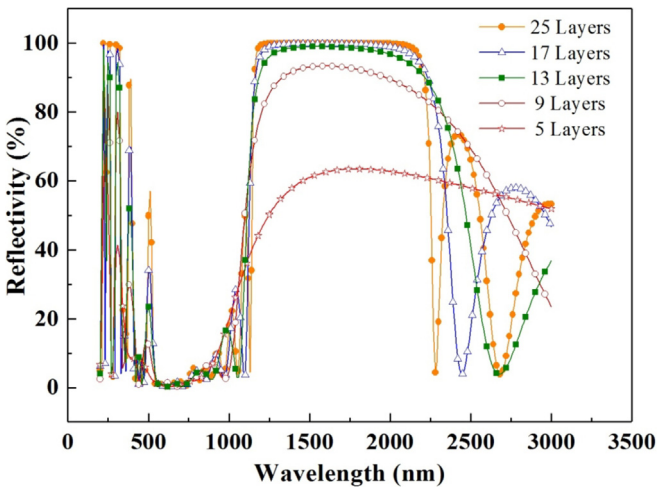


**Fig. 2.** Comparison of the design results of coating systems.

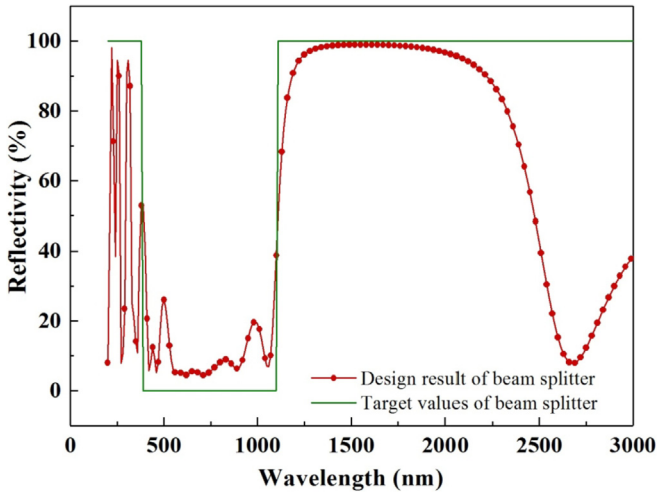


**Fig. 3.** Spectral reflectivity curve of the optimized spectral beam splitter.

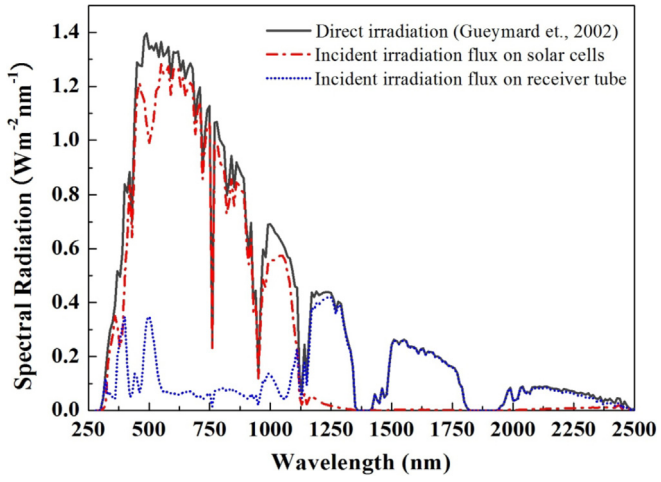


**Fig. 4.** Spectral distributions of incident irradiation flux.

splitters are shown in Fig. 3.

The spectral distributions of solar irradiation flux on the solar panel and thermal receiver tube surface after the action of the spectral beam splitter is shown in Fig. 4. The analysis results based on the curves in Fig. 4 show that the total incident irradiation flux density on the beam splitter is 900.0 W/m$^2$, and the part passing through the spectral beam splitter (or on solar cell surface) is 648.9 W/m$^2$. Hence, the average transmissivity of the beam splitter is approximately 72.1% and the average reflectivity is 27.9%. The average transmissivity and reflectivity values will be used in the following simulations and analyses.

## 3. Solar concentrating process simulation

### 3.1. Numerical method

The Monte Carlo Ray Tracing (MCRT) method is employed to simulate the solar concentrating process of the multi-segment mirror hybrid solar CPV/T system. The MCRT is a statistical method for tracking the random processes of a large number of rays [20,21]. The basic principle of MCRT method is: the solar radiation energy is assumed to be carried evenly by a great number of sample beams, and the average energy value of every beam is derived from the incident solar energy flux and the number of sample beams. Each beam would undergo optical processes, including the refraction, reflection, absorption, scattering, etc. The occurrences or non-occurrences of these optical processes are controlled by random numbers. The radiation distribution law on the solar receiving surface can be statistically obtained by tracking all the propagation processes of the sample beams.

The probabilistic model of the solar concentrator for simulation is introduced as an example in this section. Solar rays are nearly parallel but with a 32′ solid angle [21]. The coordinate systems of the incident sunlight and solar concentrator are assumed to be $o_1x_1y_1z_1$ and *OXYZ*, respectively. $y_1$-axis and *Y*-axis are parallel to each other. The angle between the incident center line of sunlight and *Z*-axis is $\delta$. If $\delta$ is equal to 0°, the concentrated light would focus on the solar cells accurately. Otherwise, the concentrated light would deviate from the solar panel. Thus, $\delta$ represents the sun tracking error of the hybrid solar CPV/T system. If the direction vector of the incident sunlight is $\boldsymbol{P}$, $\boldsymbol{A}$ is the direction vector of the sunlight reflected by the solar concentrator and $\boldsymbol{N}$ is the normal vector of the reflection flat mirror, it follows:

$$\boldsymbol{A} = \boldsymbol{P} - 2(\boldsymbol{N}\cdot\boldsymbol{P})\boldsymbol{N} \tag{13}$$

It is assumed that the distribution of incident solar energy flux density on the flat mirror is uniform and this mirror plane is the emitting surface of the sample beams. The probabilistic model of the emission point $(x_0, y_0, z_0)$ is:

$$\begin{cases} x_0 = X_L \times R_X \\ y_0 = Y_L \times R_Y - Y_L/2 \\ z_0 = Z_L \end{cases} \tag{14}$$

where $R_X$ and $R_Y$ are the random numbers of the incident light in the *X*-axis and *Y*-axis directions, and there is $R_X$ and $R_Y \in (0,1)$. $X_L$, $Y_L$ and $Z_L$ are the components of the incident point on *X*-, *Y*- and *Z*-axis, respectively.

As mentioned above, the solar rays are not absolutely parallel but with a cone angle $\theta_a$, which is equal to 16′. The solar energy density distribution in this range follows the Lambert's law. Hence, the circumferential and zenith angles perpendicular to the direction of incident solar rays could be obtained:

$$\phi = 2\pi R_\phi \tag{15}$$

$$\theta = \arcsin\sqrt{R_\theta \times \sin\left(\theta_a^2\right)} \tag{16}$$

where $R_\theta$ and $R_\varphi$ are the random numbers of the cone angle and circumference of the emitting direction, and there is $R_\theta$ and $R_\varphi \in (0,1)$. Then the direction vector of the incident ray in $o_1x_1y_1z_1$ coordinate system is:

$$\boldsymbol{P} = (\sin\theta\cos\phi, \sin\theta\sin\phi, -\cos\theta) \tag{17}$$

Using a transformation matrix *U*, the direction vector $\boldsymbol{P}^*$ of the incident ray in *OXYZ* coordinate system could be obtained:

$$\boldsymbol{P}* = U\boldsymbol{P} \tag{18}$$

where the transformation matrix *U* is as following:

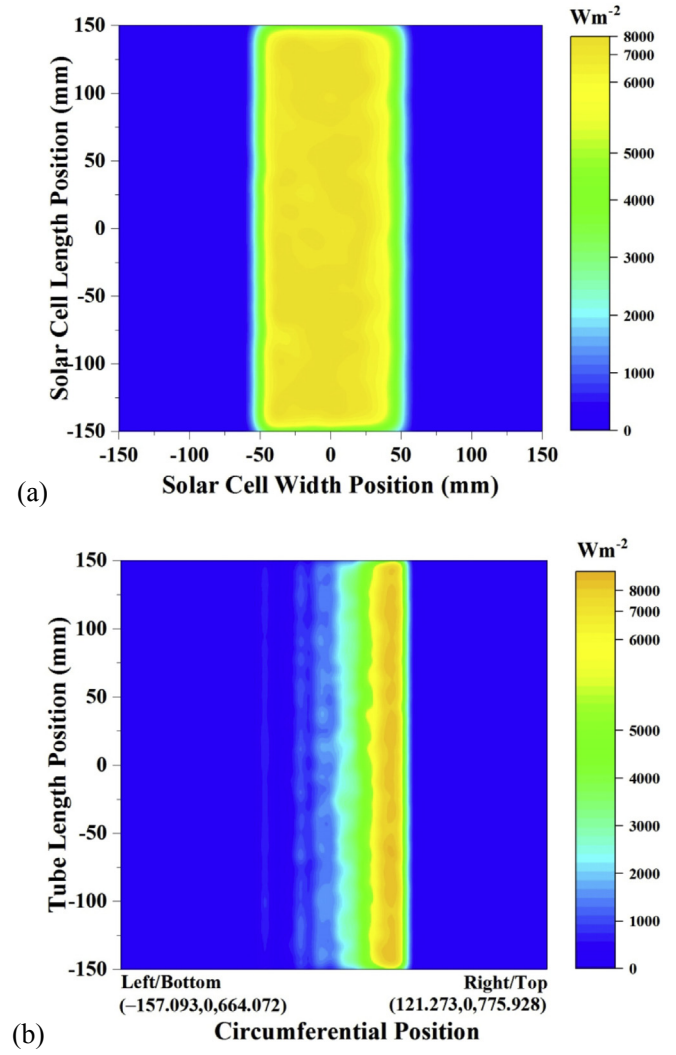


**Fig. 5.** Solar concentrating simulation results: (a) energy flux density distribution on the solar cell (b) energy flux density distribution on the receiver tube surface.

$$U = \begin{bmatrix} \cos\delta & -\sin^2\delta & \sin\delta\cos\delta \\ \sin\delta & \sin\delta\cos\delta & -\cos^2\delta \\ 0 & \cos\delta & \sin\delta \end{bmatrix} \tag{19}$$

Based on Eqs. (13)-(19), all direction vectors of incident and reflected rays on the flat mirrors could be calculated. Thus, the solar concentrating performance on the solar panel can be obtained.

### 3.2. Solar concentration simulation

For the solar concentrating simulation of the multi-segment mirror hybrid solar CPV/T system, it is assumed that the incident solar flux intensity is 1000 W m$^{-2}$ and the amount of incident rays is $10^6$. The flat mirror number $N_m$ is 15 and the tilt angle of the solar cell is 0°. The theoretical geometric concentrating ratio $CR$ is 10.41. The widths of all flat mirrors are presented in Table 1 and the mirror length is 300 mm. The reflectivity of flat mirrors is assumed to be 100%. The size of the solar cell is 100 mm × 300 mm. The transmissivity and reflectivity of the spectral beam splitter are assumed to be 72.1% and 27.9%, respectively. The diameter, length and installing height $H_t$ of the solar thermal receiver tube collector are

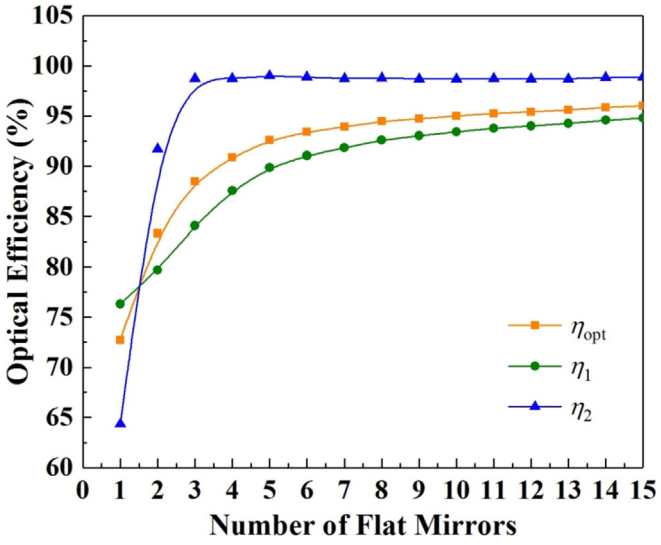


**Fig. 6.** Optical efficiencies of different parts of the hybrid solar CPV/T system.

**Table 2**
Simulation results of solar concentration process.

| $i$ | $\phi_t$/W | $CR$ | $\eta_{opt}$ | $CR_a$ | $\phi_1$/W | $\eta_1$ | $\phi_2$/W | $\eta_2$ |
|---|---|---|---|---|---|---|---|---|
| 1 | 21.605 | 0.99 | 72.74% | 0.72 | 15.87 | 76.33% | 5.735 | 64.36% |
| 2 | 49.241 | 1.97 | 83.32% | 1.64 | 32.98 | 79.71% | 16.261 | 91.71% |
| 3 | 77.238 | 2.91 | 88.47% | 2.57 | 51.38 | 84.07% | 25.858 | 98.73% |
| 4 | 103.892 | 3.81 | 90.89% | 3.46 | 70.04 | 87.54% | 33.852 | 98.72% |
| 5 | 129.176 | 4.65 | 92.60% | 4.31 | 87.74 | 89.85% | 41.436 | 99.01% |
| 6 | 152.706 | 5.45 | 93.40% | 5.09 | 104.21 | 91.05% | 48.496 | 98.87% |
| 7 | 174.407 | 6.19 | 93.92% | 5.81 | 119.40 | 91.85% | 55.007 | 98.74% |
| 8 | 194.691 | 6.87 | 94.47% | 6.49 | 133.60 | 92.60% | 61.091 | 98.80% |
| 9 | 213.422 | 7.51 | 94.73% | 7.11 | 146.71 | 93.03% | 66.712 | 98.70% |
| 10 | 230.884 | 8.10 | 95.02% | 7.70 | 158.93 | 93.43% | 71.954 | 98.70% |
| 11 | 246.914 | 8.64 | 95.26% | 8.23 | 170.15 | 93.78% | 76.764 | 98.72% |
| 12 | 261.631 | 9.14 | 95.42% | 8.72 | 180.45 | 94.01% | 81.181 | 98.69% |
| 13 | 275.286 | 9.60 | 95.59% | 9.18 | 190.01 | 94.25% | 85.276 | 98.70% |
| 14 | 288.171 | 10.02 | 95.87% | 9.61 | 199.03 | 94.59% | 89.141 | 98.85% |
| 15 | 299.870 | 10.41 | 96.02% | 10.00 | 207.22 | 94.79% | 92.650 | 98.89% |

100 mm, 300 mm and 720 mm. A secondary reflector is employed. The simulation results are presented in Figs. 5 and 6 and Table 2.

Fig. 5(a) and (b) show the solar concentration simulation performances on the solar panel and the surface of receiver tube, respectively. It is clear that the concentrated solar radiation on surface of the solar panel has a relatively high uniformity, which is consistent with the design goal of uniform solar concentration in this study. The radiation uniformity on the surface of receiver tube is low.

In Fig. 6 and Table 2, $\varphi_1$ and $\varphi_2$ are the radiation flux values incident on the solar panel and receiver tube collector surface, respectively. $\varphi_t$ is the sum of $\varphi_1$ and $\varphi_2$. $\eta_1$ and $\eta_2$ are the optical efficiencies of the solar cell and solar collector parts, respectively. $\eta_{opt}$ is the overall optical efficiency of the whole CPV/T system. $CR_a$ represents the actual geometric concentration ratio of the CPV/T system and could be expressed as:

$$CR_a = \eta_{opt} \cdot CR \tag{20}$$

As shown in Fig. 6 and Table 2, the optical efficiency of solar cell part and overall optical efficiency both increase with the flat mirror number $N_m$ increased. The optical efficiency of solar thermal receiver tube part increases first and then reaches the maximum

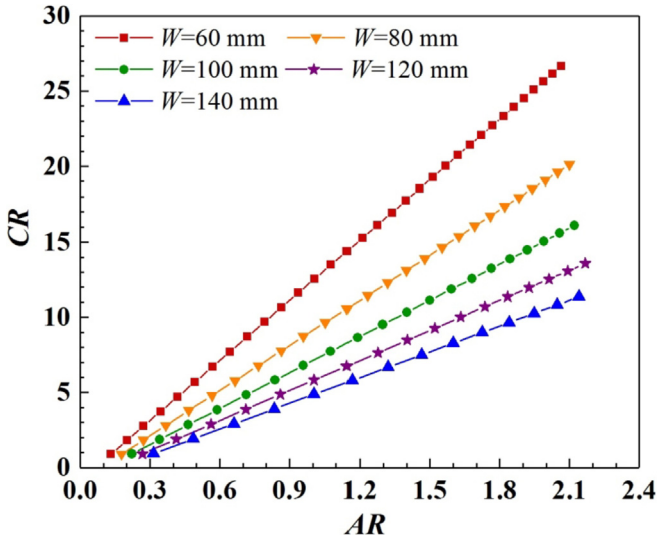


**Fig. 7.** Relationship of *AR*, *CR* and *W* ($\alpha = 30°$, $H_M = 800$ mm).

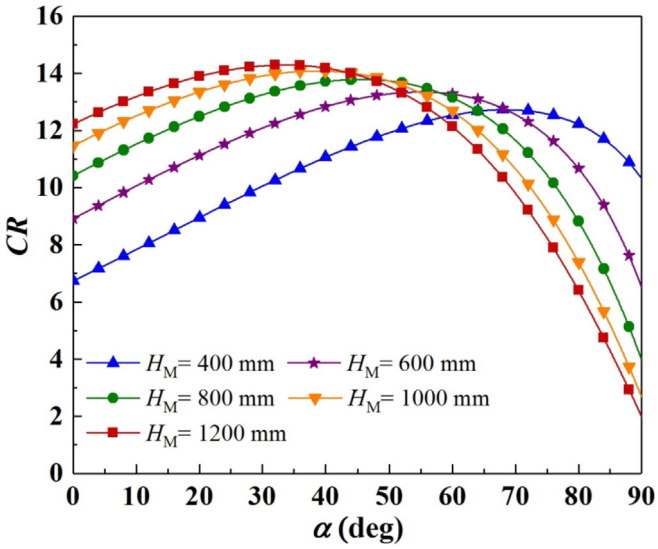


**Fig. 9.** Relationship of *CR*, $\alpha$ and $H_M$ ($W = 100$ mm, $N_m = 15$).

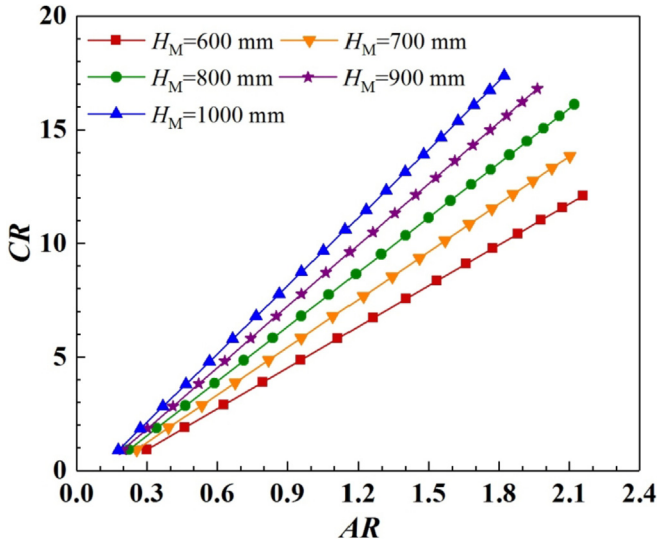


**Fig. 8.** Relationship of *AR*, *CR* and $H_M$ ($\alpha = 30°$, $W = 100$ mm).

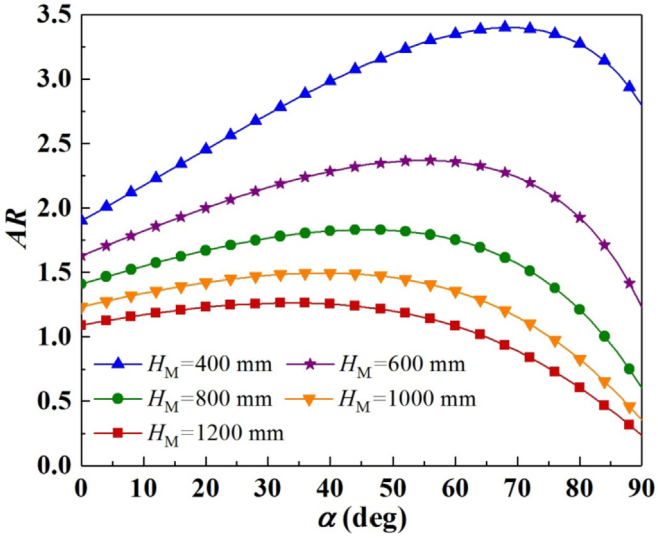


**Fig. 10.** Relationship of *AR*, $\alpha$ and $H_M$ ($W = 100$ mm, $N_m = 15$).

value of 99.01%. After that, it fluctuates slightly around 98.80% with the increasing of the flat mirror number $N_m$. For the hybrid solar CPV/T system with 15 flat mirrors, the theoretical total radiation flux incident on the solar panel surface should be 218.61 W, and the simulation result is about 207.22 W. Hence, $\eta_1$ is approximately 94.79%. The incident radiation flux on the surface of thermal receiver tube collector is about 92.65 W, but the theoretical radiation flux reflected by the spectral beam splitter should be 93.69 W. Thus, $\eta_2$ and $\eta_{opt}$ are 98.89% and 96.02%, respectively.

## 4. Optical analysis

The parameter effect analyses are carried out to investigate the interactions of the key structural and optical parameters of the proposed CPV/T system. When the installing height $H_M$ and the tilt angle $\alpha$ of solar cells are 800 mm and 30°, the relationship of the theoretical geometric concentrating ratio *CR*, relative aperture *AR* and solar cell width *W* is presented in Fig. 7. The results indicate that when *W* is unchanged, *CR* increases linearly with the increasing of *AR*. For the same relative aperture *AR*, *CR* decreases with the increasing of *W*.

Assuming the tilt angle $\alpha$ of solar panel is 30° and the solar cell width *W* is 100 mm, for different $H_M$ values, the relationship between the theoretical geometric concentration ratio *CR* and relative aperture *AR* is shown in Fig. 8. Similarly, when $H_M$ is unchanged, *CR* also increases linearly with the increasing of *AR*. But when *AR* is unchanged, *CR* increases with $H_M$ increased. Thus, a large solar cell installing height would result in a large theoretical geometric concentrating ratio. In practical applications, the design value of $H_M$ should be taken into a comprehensive consideration, as a larger solar cell installing height would also lead to more light loss and a larger wind load [22].

When the solar cell width *W* is 100 mm and the flat mirror number $N_m$ is 15, for different solar cell installing heights, the relationship between the theoretical geometric concentrating ratio *CR* and the solar cell tilt angle $\alpha$ is shown in Fig. 9. As shown in

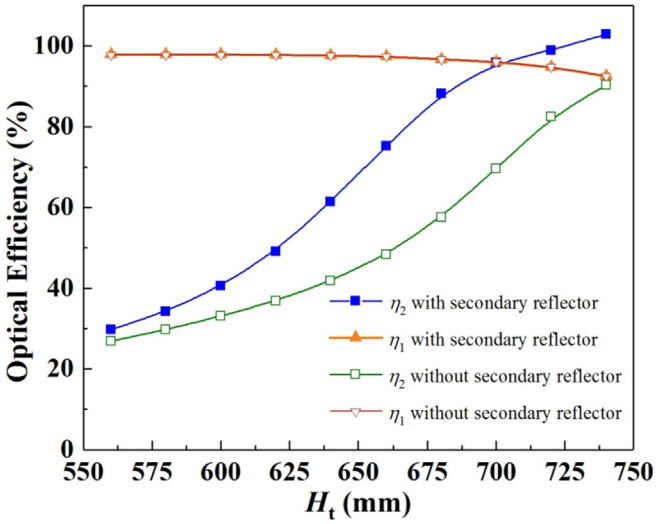


**Fig. 11.** Relationship of $\eta_1$, $\eta_2$ and $H_t$.

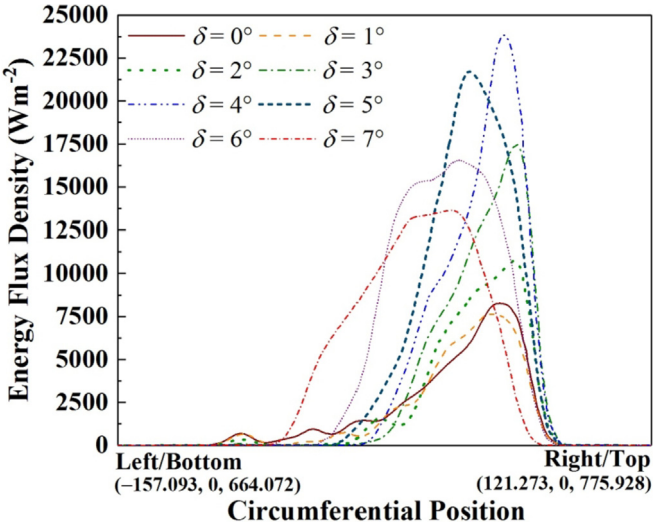


**Fig. 13.** Radiation flux density distributions on the receiver tube surface under different sun tracking errors.

Fig. 9, for different installing heights of the solar panel, with the increasing of the solar cell tilt angle $\alpha$ from 0° to 90°, the theoretical geometric concentrating ratios all increase first and then decrease after reaching the maximum values.

The relationship of the relative aperture *AR*, solar panel tilt angle $\alpha$ and solar cell installing height $H_M$ is presented in Fig. 10. When the solar cell installing height is unchanged, the relative aperture *AR* increases first with $\alpha$ increased from 0° to 90°, then decreases after reaching the peak value. At different solar cell tilt angles, the relative apertures all decrease with the increasing of solar cell installing height $H_M$.

The installing height $H_t$ of thermal receiver tube is important for the collection of the solar radiation reflected by the beam filter. Hence, the optical efficiencies of different parts of the proposed CPV/T system at different receiver tube installing heights are calculated and the results are shown in Fig. 11. Two conditions are considered, which are with and without the secondary reflector. The receiver tube diameter and the solar panel installing height $H_M$ are assumed to be 100 mm and 800 mm, respectively. The results show that with $H_t$ increasing from 550 mm to 750 mm, the optical efficiency of receiver tube part increases, but the optical efficiency of solar cell part keeps unchanged first and then decreases slightly. The optical efficiency of receiver tube with the secondary reflector is higher than that of the tube without the secondary reflector. The optical efficiency values of solar cell part are the same under the two different conditions.

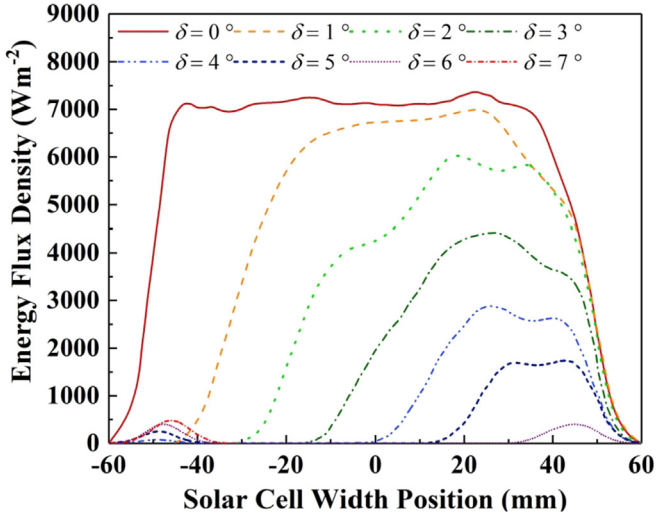


**Fig. 12.** Radiation flux density distributions on the solar panel under different sun tracking errors.

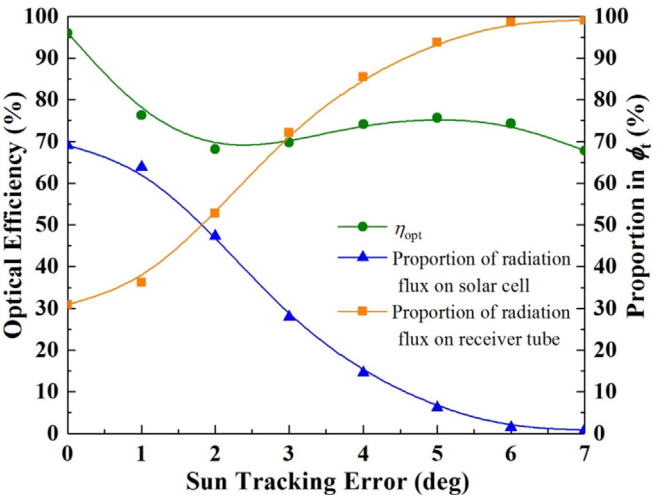


**Fig. 14.** Sun tracking error effect on the overall optical efficiency of the hybrid solar CPV/T system.

## 5. Sun tracking error effect analysis

The deviation angle $\delta$ could be used to judge the sun tracking error of the multi-segment mirror hybrid solar CPV/T system. If the deviation angle $\delta$ is 0°, the incident solar rays will be accurately reflected to the default position by the flat mirrors. Otherwise, the reflected solar rays will deviate from the preset positions and the solar radiation distributions on solar cells and receiver tube collector will also change. When *CR* is 10.41 and *AR* is 1.41, the sun

tracking error effect is investigated and the results are presented in Figs. 12–14.

Figs. 12 and 13 show the solar radiation flux density distributions on the solar panel and receiver tube surface under different tracking errors, respectively. The results indicate that for the solar panel, with the increasing of deviation angle $\delta$, the radiation flux density decreases and the concentrated radiation uniformity becomes lower and lower. When the deviation $\delta$ is increased to 7°, the radiation flux on the solar panel is only 1.9 W. For the solar thermal receiver tube, with the increasing of $\delta$, the radiation flux increases first and reaches the maximum value of 228.91 W at $\delta$ of 6°, then decreases slightly.

The relationship between the overall optical efficiency $\eta_{opt}$ of the proposed CPV/T system and the sun tracking error is shown in Fig. 14. And the proportions of radiation flux on the solar panel and receiver tube in total radiation flux $\varphi_t$ under different sun tracking errors are also presented in Fig. 14. When the deviation angle $\delta$ is 1°, the overall optical efficiency $\eta_{opt}$ decreases to 76.3%, and the proportions of the radiation flux on the solar cell and receiver tube are 63.8% and 36.2%, respectively. At $\delta$ of 7°, though the overall optical efficiency $\eta_{opt}$ is still 67.83%, the proportion of the radiation flux on the receiver tube increases to 99.1%. That means almost all the solar energy is receiving by the solar thermal receiver tube collector. As the sun tracking error is normally less than 1°, it can be concluded that the CPV/T system could keep an overall optical efficiency higher than 76.3% in practical applications.

## 6. Thermodynamic analysis

### 6.1. PV conversion

Normally, the output power of a solar cell follows a current-voltage curve and has the maximum value around the knee in the curve where the voltage begins to drop off significantly as the current draw is increased. For the multi-segment mirror hybrid solar CPV/T system, the maximum power generated by solar cells could be expressed as:

$$P_{PV,C,bs,m} = V_{C,bs,m} \cdot I_{C,bs,m} \tag{21}$$

where $V_{C,bs,m}$ and $I_{C,bs,m}$ are the voltage and current values at the maximum power point of the I-V curve of the solar cells under solar concentration and beam splitting condition, respectively.

The open circuit voltage under spectral beam splitting waveband of $\lambda_1$~$\lambda_2$ could be approximately expressed as [17]:

$$V_{OC,C,bs} = \frac{hc}{\lambda_2} \cdot \frac{V_{OC}}{E_g} + \frac{n_f k T_{cell}}{e} \ln(CR) \tag{22}$$

where $V_{OC}$ is the open circuit voltage of the solar cell under 1 × SUN illumination condition. $e$ is the charge of an electron, $n_f$ is the diode ideality factor, $T_{cell}$ is the operating temperature of solar cell, $h$ is the Planck constant, and $c$ is the velocity of light in the vacuum. $E_g$ is the bandgap energy of solar cell. $k$ is the Boltzmann constant and equal to $1.38065 \times 10^{-23}$ $m^2 kg \cdot s^{-2} K^{-1}$. And the thermal voltage $V_{th}$ can be expressed as:

$$V_{th} = \frac{n_f k T_{cell}}{e} \tag{23}$$

Theoretically, the short circuit current of the solar cell under solar concentration and beam splitting condition is linear with $CR$ [11], and there should be:

$$I_{SC,C,bs} = CR \cdot I_{SC,bs} \tag{24}$$

where $I_{SC,bs}$ is the short circuit current of the solar cell under 1 × SUN illumination and beam splitting condition. After the action of the beam splitter designed in this study, $I_{SC,bs}$ should be:

$$I_{SC,bs} = \int_0^\infty \rho_m(\lambda) \cdot \tau(\lambda) \cdot E(\lambda) \cdot QE(\lambda) \cdot \frac{e\lambda}{hc} \cdot A_{cell} d\lambda \tag{25}$$

where $\rho_m(\lambda)$ is spectral reflectivity of flat mirrors, $\tau(\lambda)$ is the spectral transmissivity of the beam filter, $QE(\lambda)$ is the spectral external quantum efficiency of the solar cell, and $A_{cell}$ is the total area of the solar cells.

For the calculation of fill factor $FF$, a common empirical formula of $FF$ is given as [23]:

$$FF = \frac{v_{oc} - \ln(v_{oc} + 0.72)}{1 + v_{oc}} (1 - r_s) \tag{26}$$

where $v_{oc}$ is the open circuit voltage normalized to $V_{th}$. $r_s$ is the actual solar cell series resistance $R_s$ normalized to the characteristic resistance $R_{ch}$ of solar cell. For the hybrid solar CPV/T system, $R_{ch}$ is $V_{OC,C,bs}/I_{SC,C,bs}$.

The PV conversion efficiency of the CPV/T system is:

$$\eta_{PV} = \frac{P_{PV,C,bs,m}}{q_{PV,bs}} \tag{27}$$

where $q_{PV,bs}$ is the solar energy flux delivered to solar panel by the spectral beam splitter. It can be expressed as:

$$q_{PV,bs} = q_{in} \int_0^\infty \rho_m(\lambda) \tau(\lambda) d\lambda \tag{28}$$

where $q_{in}$ is the incident solar energy flux on the solar concentrator.

For a CPV system without the spectral beam splitter, the relative formulas are as follows:

$$P_{PV,C,m} = V_{C,m} \cdot I_{C,m} \tag{29}$$

$$V_{OC,C} = V_{OC} + \frac{n_f k T_{cell}}{e} \ln(CR) \tag{30}$$

$$I_{SC,C} = CR \int_0^\infty \rho_m(\lambda) \cdot E(\lambda) \cdot QE(\lambda) \cdot \frac{e\lambda}{hc} \cdot A_{cell} d\lambda \tag{31}$$

$$q_{PV} = q_{in} \int_0^\infty \rho_m(\lambda) d\lambda \tag{32}$$

$$\eta_{PV} = \frac{P_{PV,C,m}}{q_{PV}} \tag{33}$$

where $P_{PV,C,m}$, $V_{C,m}$, $I_{C,m}$ are the maximum output power and its corresponding voltage and current values of the solar cells used in the CPV system, respectively.

### 6.2. Thermal utilization

The solar energy delivered to the thermal receiver tube by the

spectral beam splitter could be used in many applications. In this study, to compare with the CPV system more conveniently, the thermal receiver tube is assumed to be used as the high temperature source of a heat engine. The solar energy absorbed by the receiver tube is used to generate power. The solar energy flux delivered to the receiver tube $q_{th}$ is:

$$q_{th} = q_{in}\int_0^{\infty} \rho_m(\lambda)\rho(\lambda)d\lambda \tag{34}$$

Assuming the operating temperature of the solar thermal receiver tube collector is $T_t$, the solar energy flux absorbed by the tube collector is $q_a$, the radiation loss of the tube collector is $q_{loss}$, and the convection loss of the tube collector is neglected, the thermal efficiency of the tube collector is:

$$\eta_{th} = \frac{q_{net}}{q_{th}} = \frac{q_a - q_{loss}}{q_{th}} \tag{35}$$

where $q_{net}$ is the net heat flux transferred to the heat engine. For the middle temperature solar thermal receiver, there should be:

$$q_a = q_{in}\int_0^{\infty} \tau_{shell}(\lambda)\rho_m(\lambda)\rho(\lambda)\alpha_t(\lambda)d\lambda \tag{36}$$

$$q_{loss} = \varepsilon \cdot A_{th}\int_0^{\infty} E_{b,\lambda,T}d\lambda \tag{37}$$

where $\alpha_t(\lambda)$, $\varepsilon$ and $A_t$ are the spectral absorptivity, average emissivity and surface area of the receiver tube, respectively. $\tau_{shell}$ is the spectral transimissivity of the receiver tube shell. $\rho(\lambda)$ is the spectral reflectivity of the beam splitter. $E_{b,\lambda,T}$ is the spectral radiation of the blackbody with the temperature of $T_t$. Thus, the power generated by the heat engine is:

$$P_{th} = \eta_{t,ex}\cdot q_{net}\left(1-\frac{T_0}{T_t}\right) = \eta_{t,ex}\cdot\eta_{th}\cdot q_{th}\left(1-\frac{T_0}{T_t}\right) \tag{38}$$

where $T_0$ is the ambient temperature and $\eta_{t,ex}$ is the exergy efficiency of the thermal power sub-system.

Hence, the total power generated by the CPV/T system is:

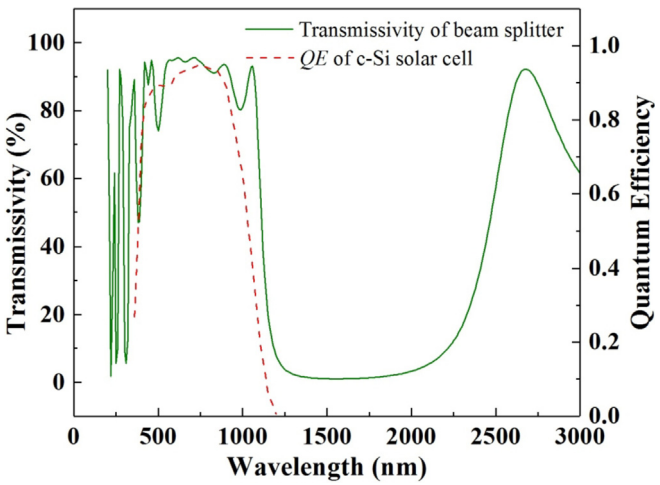


**Fig. 15.** Spectral transmissivity curve of the beam splitter and *QE* of the c-Si solar cell.

**Table 3**
Comparison of thermodynamic analysis results of the CPV/T and CPV systems.

| Parameters | CPV/T system | CPV system |
|---|---|---|
| $q_{in}$ | 5472.0 W | 5472.0 W |
| $q_{PV,bs}$ or $q_{PV}$ | 3748.0 W | 5198.4 W |
| $q_t$ | 1450.4 W | – |
| $P_{PV,C,bs,m}$ or $P_{PV,C,m}$ | 1155.0 W | 1271.7 W |
| $P_{th}$ | 254.8 W | – |
| $P_{total}$ | 1409.8 W | 1271.7 W |
| $\eta_{PV}$ | 30.8% | 24.5% |
| $\eta_{th}$ | 73.0% | – |
| $\eta_{sys}$ | 25.8% | 23.2% |

$$P_{total} = P_{PV,C,bs,m} + P_{th} \tag{39}$$

The overall energy efficiency of the proposed CPV/T system is:

$$\eta_{sys} = \frac{P_{total}}{q_{in}} = \frac{P_{PV,C,bs,m} + P_{th}}{q_{in}} \tag{40}$$

### 6.3. Comparison analysis

In this comparison analysis, the beam splitter design is introduced in Section 2.2 and the c-Si solar cell is assumed to be used in the hybrid solar CPV/T system. The spectral transmissivity of the beam splitter and the $QE(\lambda)$ curve of c-Si solar cell [17] are shown in Fig. 15. The spectral beam splitting waveband is 380 nm–1100 nm. The proposed CPV/T system with $\alpha$ of 30° and $H_M$ of 1500 mm is taken for example in this section. The width of the solar cell is 100 mm and the length of the flat mirror is assumed to be 2000 mm. The solar concentrator is comprised of 38 flat mirrors and the theoretical geometric concentrating ratio *CR* is 30.4. The direct incident solar radiation flux intensity is 900 W $m^{-2}$ with AM 1.5D spectrum. Thus, the total incident solar radiation flux $q_{in}$ on the solar concentrator is 5472.0 W. The open circuit voltage $V_{OC}$ and fill factor *FF* of the c-Si solar cell under standard test conditions are 0.706 V and 0.828 [24]. The diode ideality factor $n_f$ and normalized series resistance $r_s$ of the c-Si solar cell are 1.28 and 0.012 [11]. The operating temperature $T_{cell}$ of the solar cells is assumed to be 30 °C. For the CPV system, all the initial conditions and assumptions are the same except that the beam splitter and thermal utilization system are not employed. By using Eqs. (21)-(33), the powers and photo-electric conversion efficiencies of PV conversion parts of both the CPV/T and CPV systems can be calculated.

For the thermal utilization of the proposed CPV/T system, the operating temperature $T_t$ of the solar thermal receiver tube and the ambient temperature $T_0$ are assumed to be 300 °C and 25 °C, respectively. According to Eq. (34), the solar energy flux delivered to the receiver tube $q_{th}$ is 1450.4 W. When the operating temperature of the receiver tube is less than 350 °C, the emissivity $\varepsilon$ of the receiver tube is about 0.15 [11]. The exergy efficiency $\eta_{t,ex}$ of the thermal power sub-system is assumed to be 0.5 [25]. By using Eqs. (35)-(40), the power $P_{th}$ generated by the thermal power sub-system and the overall energy efficiency $\eta_{sys}$ of the CPV/T system could be obtained. All of the calculation results are presented in Table 3. As shown in Table 3, the powers generated by the solar cells and thermal power sub-system of the proposed CPV/T system are 1155.0 W and 254.8 W, respectively. The PV conversion efficiency and overall energy efficiency of the proposed CPV/T system are 30.8% and 25.8%, which are both higher than those of the CPV system without the spectral beam splitter.

## 7. Conclusions

A novel multi-segment mirror hybrid solar CPV/T system with spectral beam splitter is proposed. The components and design principles of the CPV/T system are introduced. The spectral beam splitter design is optimized by using the Needle optimization method. The beam splitter has a high transmissivity in the spectral range from 380 nm to 1100 nm and a relatively high reflectivity for other wavelengths. The MCRT method is used to simulate the solar concentrating processes of the proposed CPV/T system. The simulation results reveal that the uniformity of solar energy flux density distribution on the solar panel is high. The relationships of key structural and optical parameters of the CPV/T system are analyzed. The results show that a large installing height and a small width of solar cell are good for increasing the geometric concentrating ratio. When the solar cell width, solar cell installing height and flat mirror number are unchanged, the geometric concentrating ratio has peak values with the increasing of solar cell tilt angle from 0° to 90°. The sun tracking error effect on the solar concentrating performance of the CPV/T system is carried out. The analysis results indicate that the system has an overall optical efficiency higher than 76.3% when the sun tracking error is less than 1°. Furthermore, the thermodynamic analysis of the proposed CPV/T system is conducted and the results are compared with those of the CPV system without the spectral beam splitter. The comparison results reveal that the PV conversion efficiency and overall energy efficiency of the CPV/T system are both higher than those of the CPV system under the same condition.

## References


[1] Abid M, Ratlamwala TAH, Atikol U. Performance assessment of parabolic dish and parabolic trough solar thermal power plant using nanofluids and molten salts. Int J Energy Res 2016;40:550–63.
[2] Singh GK. Solar power generation by PV (photovoltaic) technology: a review. Energy 2013;53:1–13.
[3] Siddiqui R, Kumar R, Jha GK, et al. Comparison of different technologies for solar PV (Photovoltaic) outdoor performance using indoor accelerated aging tests for long term reliability. Energy 2016;107:550–61.
[4] Luque A, Sala G, Luque-Heredia I. Photovoltaic concentration at the onset of its commercial deployment. Prog Photovoltaics Res Appl 2006;14(5):413–28.
[5] Wang G, Chen Z, Hu P, et al. Design and optical analysis of the band-focus Fresnel lens solar concentrator. Appl Therm Eng 2016;102:695–700.
[6] Baharoon DA, Rahman HA, Omar WZW, et al. Historical development of concentrating solar power technologies to generate clean electricity efficiently-A review. Renew Sustain Energy Rev 2015;41:996–1027.
[7] Wang G, Chen Z, Hu P. Design and experimental investigation of a multi-segment plate concentrated photovoltaic solar energy system. Appl Therm Eng 2017;108:147–52.
[8] Luque A, Sala G, Arboiro JC. Electric and thermal model for non-uniformly illuminated concentration cells. Sol Energy Mater Sol Cells 1998;51:269–90.
[9] Ryu K, Rhee JG, Park KM, et al. Concept and design of modular Fresnel lenses for concentration solar PV system. Sol Energy 2006;80:1580–7.
[10] Jiang S, Hu P, Mo S, et al. Optical modeling for a two-stage parabolic trough concentrating photovoltaic/thermal system using spectral beam splitting technology. Sol Energy Mater Sol Cells 2010;94(10):1686–96.
[11] Liu Y, Hu P, Zhang Q, et al. Thermodynamic and optical analysis for a CPV/T hybrid system with beam splitter and fully tracked linear Fresnel reflector concentrator utilizing sloped panels. Sol Energy 2014;103:191–9.
[12] Ju X, Xu C, Han X, et al. A review of the concentrated photovoltaic/thermal (CPVT) hybrid solar systems based on the spectral beam splitting technology. Appl Energy 2017;187:534–63.
[13] Algareu AO, Mahmoud S, Al-Dadah RK. Electrical characterization of photovoltaic cell with low-concentration ratio square aperture concentrator. Int J Energy Res 2017:1–13.
[14] Lasich JB, Cleeve A, Kaila N, et al. Close-packed cell arrays for dish concentrators. In: IEEE first world conference on photovoltaic energy conversion, Hawaii, USA, December 5–9, 1994; 1994.
[15] Crisostomo F, Becker J, Mesgari S, et al. Design and on-sun testing of a hybrid PVT prototype using a nanofluid-based selective absorption filter. 12th International conference on the European energy market, Lisbon, Portugal, May 19–22, 2015.
[16] Imenes AG, Mills DR. Spectral beam splitting technology for increased conversion efficiency in solar concentrating systems: a review. Sol Energy Mater Sol Cells 2004;84:19–69.
[17] Ju X, Wang Z, Flamant G, et al. Numerical analysis and optimization of a spectrum splitting concentration photovoltaic-thermoelectric hybrid system. Sol Energy 2012;86:1941–54.
[18] Verly PG. Modified needle method with simultaneous thickness and refractive-index refinement for the synthesis of inhomogeneous and multilayer optical thin films. Appl Opt 2001;40(31):5718–25.
[19] Tikhonravov AV, Trubetskov MK. Application of the needle optimization technique to the design of optical coatings. Appl Opt 1996;35(28):5493–508.
[20] Cheng ZD, He YL, Cui FQ. A new modelling method and unified code with MCRT for concentrating solar collectors and its applications. Appl Energy 2013;101:686–98.
[21] Cheng ZD, He YL, Cui FQ, et al. Comparative and sensitive analysis for parabolic trough solar collectors with a detailed Monte Carlo ray-tracing optical model. Appl Energy 2014;115:559–72.
[22] Zhu J, Chen Z. Optical design of compact linear fresnel reflector systems. Sol Energy Mater Sol Cells 2018;176:239–50.
[23] Green MA. Solar cell fill factors: general graph and empirical expressions. Solid State Electron 1981;24(8):788–9.
[24] Green MA, Emery K, Hishikawa Y, et al. Solar cell efficiency tables (version 42). Prog Photovoltaics Res Appl 2013;21:827–37.
[25] El-Emam RS, Dincer I. Exergy and exergoeconomic analyses and optimization of geothermal organic Rankine cycle. Appl Therm Eng 2013;59:435–44.


## Nomenclature

***A***: direction vector of the sunlight reflected by the solar concentrator (−)
$A_{cell}$: total area of solar cells ($m^2$)
$A_{th}$: surface area of the receiver tube ($m^2$)
*AR:* relative aperture (−)
*c:* velocity of light in the vacuum (m/s)
*CR:* theoretical geometric concentration ratio (−)
$CR_a$: actual geometric concentration ratio (−)
$E_{b,\lambda,T}$: spectral radiation of the blackbody ($Wm^{-2}nm^{-1}$)
$E_g$: bandgap energy of the solar cells (eV)
*e:* charge of an electron (C)
*FF:* fill factor (−)
*h:* Planck constant (J·s)
$H_M$: installing height of the solar cell (mm)
$H_t$: installing height of the solar thermal receiver tube (mm)
$I_{SC}$: short circuit current (A)
*K:* slope of a flat mirror (−)
*k:* Boltzmann constant ($m^2kg \cdot s^{-2}K^{-1}$)
*L:* width of a flat mirror (mm)
***N***: normal vector of the reflection flat mirror (−)
$N_m$: number of flat mirrors (−)
$n_f$: diode ideality factor (−)
***P***: direction vector of the incident sunlight (−)
$P_{PV,C,m}$: maximum power generated by the solar cells of the CPV system (W)
$P_{PV,C,bs,m}$: maximum power generated by the solar cells of the hybrid solar CPV/T system (W)
$P_{th}$: power generated by the thermal power sub-system (W)
$P_{total}$: total power generated by the hybrid solar CPV/T system (W)
*QE:* spectral external quantum efficiency of solar cells (−)
$q_a$: solar energy flux absorbed by the receiver tube (W)
$q_{in}$: incident solar energy flux on the solar concentrator (W)
$q_{loss}$: radiation loss of the thermal receiver (W)
$q_{net}$: net heat flux transferred to the heat engine (W)
$q_{th}$: solar energy flux delivered to the receiver tube (W)
$q_{PV,bs}$: solar energy flux delivered to solar cells by the beam splitter (W)
*R:* random number (−)
$r_s$: actual solar cell series resistance normalized to the characteristic resistance of solar cells (−)
$T_0$: ambient temperature (°C)
$T_{cell}$: operating temperature of solar cells (°C)
$T_t$: operating temperature of the thermal receiver tube (°C)
*U:* transformation matrix (−)
$V_{th}$: thermal voltage (V)
$V_{OC}$: open circuit voltage (V)
$v_{oc}$: open circuit voltage normalized to the thermal voltage (−)
*W:* width of the solar cell (mm)

*Greek symbols*

$\alpha$: tilt angle of the solar cell (deg)
$\alpha_t$: spectral absorptivity of the receiver tube (−)
$\beta$: tilt angle of a flat mirror (deg)
$\delta$: deviation angle (deg)
$\varepsilon$: average emissivity of the receiver tube (−)
$\eta_1$: optical efficiency of the solar cell part (−)
$\eta_2$: optical efficiency of the solar collector part (−)
$\eta_{opt}$: overall optical efficiency of the CPV/T system (−)
$\eta_{t,ex}$: exergy efficiency of the thermal power sub-system (−)
$\eta_{th}$: thermal efficiency of the receiver tube (−)

$\eta_{PV}$: PV conversion efficiency (−)
$\eta_{sys}$: overall energy efficiency of the CPV/T system (−)
$\theta$: zenith angle perpendicular to the direction of incident solar rays (deg)
$\theta_a$: cone angle of the solar rays (deg)
$\lambda$: wavelength of solar radiation (nm)
$\rho$: spectral reflectivity of the beam splitter (−)
$\rho_m$: spectral reflectivity of flat mirrors (−)
$\tau$: spectral transmissivity of the beam splitter (−)
$\tau_{shell}$: transimissivity of the receiver tube shell (−)
$\varphi_1$: radiation flux incident on the solar panel surface (W)
$\varphi_2$: radiation flux incident on the receiver tube surface (W)
$\varphi_t$: sum of the radiation fluxes incident on the solar panel and receiver tube surfaces (W)
$\varphi$: circumferential angle perpendicular to the direction of incident solar rays (deg)

*Subscripts*

*bs:* beam splitting condition
*C:* solar concentration condition
*cell:* solar cell
*i:* serial number of a flat mirror